

# Characterization of the nuclei identification performances of the plastic scintillator detector prototype for the future HERD satellite experiment

D. Serini<sup>†</sup>, C. Altomare<sup>\*†</sup>, F. Alemanno<sup>§¶</sup>, N. Aprile Ximenes<sup>†</sup>, F.C.T. Barbato<sup>§¶</sup>, P. Bernardini<sup>\*\*††</sup>, I. Cagnoli<sup>§¶</sup>, E. Casilli<sup>\*\*††</sup>, P.W. Cattaneo<sup>||</sup>, A. Comerma<sup>‡‡x</sup>, I. De Mitri<sup>§¶</sup>, F. de Palma<sup>\*\*††</sup>, C. De Vecchi<sup>||</sup>, A. Di Giovanni<sup>§¶</sup>, L. Di Venere<sup>†</sup>, M. Di Santo<sup>§¶</sup>, A. Espinya<sup>‡‡</sup>, M. Fernandez Alonso<sup>§¶</sup>, G. Fontanella<sup>§¶</sup>, P. Fusco<sup>†‡</sup>, F. Gargano<sup>†</sup>, D. Gascon<sup>‡‡</sup>, S. Gomez<sup>‡‡x</sup>, D. Guberman<sup>‡‡</sup>, D. Kyrtzsis<sup>§¶</sup>, F. Licciulli<sup>†</sup>, F. Loparco<sup>†‡</sup>, S. Loporchio<sup>†‡</sup>, L. Lorusso<sup>†‡</sup>, M.N. Mazziotta<sup>†</sup>, M. Mongelli<sup>†</sup>, J. Mauricio<sup>‡‡</sup>, A. Parenti<sup>§¶</sup>, G. Panzarini<sup>†‡</sup>, R. Pillera<sup>†‡</sup>, A. Rappoldi<sup>||</sup>, G. Raselli<sup>||</sup>, M. Rossella<sup>||</sup>, A. Sammukh<sup>‡‡</sup>, A. Sanuy<sup>‡‡</sup>, A. Smirnov<sup>§¶</sup>, L. Silveri<sup>§¶</sup>, A. Surdo<sup>\*\*</sup>, R. Triggiani<sup>†</sup>, L. Wu<sup>§¶</sup>  
*on behalf of the HERD collaboration*

<sup>†</sup>INFN Sezione di Bari, 70125 Bari, Italy

<sup>‡</sup>Dipartimento Interateneo di Fisica dell'Università e del Politecnico di Bari, 70126 Bari, Italy

<sup>§</sup>Gran Sasso Science Institute (GSSI), L'Aquila, Italy

<sup>¶</sup>Istituto Nazionale di Fisica Nucleare (INFN)—Laboratori Nazionali del Gran Sasso, L'Aquila, Italy

<sup>||</sup>Istituto Nazionale di Fisica Nucleare (INFN)—Sezione di Pavia, Italy

<sup>\*\*</sup>Dipartimento di Matematica e Fisica "Ennio de Giorgi", Università del Salento, Italy

<sup>††</sup>Istituto Nazionale di Fisica Nucleare (INFN)—Sezione di Lecce, Italy

<sup>‡‡</sup>Institute of Cosmos Sciences - University of Barcelona (ICC-UB), Barcelona, Spain

<sup>x</sup>Serra Húnter Fellow, Polytechnic University of Catalonia (UPC), Barcelona, Spain

<sup>\*</sup>Corresponding authors, email: davide.serini@ba.infn.it, corrado.altomare@ba.infn.it

**Abstract**—Satellite experiments employ plastic scintillators to discriminate charged from neutral particles and to identify charged nuclei. We have assembled and tested a prototype of Plastic Scintillator Detector (PSD) equipped with Silicon Photomultipliers (SiPMs) for the High Energy Cosmic Radiation Detection facility (HERD) that will be installed onboard the future Chinese Space Station (CSS). The HERD experiment will provide high quality data on charged cosmic rays up to PeV energies and gamma rays above 100 MeV energies. In order to explore the capability of charge identification of nuclei up to iron, a beam test campaign was performed in 2022 at CERN to study the overall performance of the PSD. The PSD prototype is composed of 8 plastic scintillator trapezoidal bars of two different lengths. The PSD prototype was irradiated with an ion beam composed of particles of selected momentum of 150 GeV/n at CERN SPS H8 beam line. Along the beam line two  $10 \times 10 \times 0.5$  cm<sup>3</sup> squared plastic scintillator tiles were also placed to monitor the beam composition and the particle fragmentation upstream and downstream the beam line. In this work the main results of the SPS H8 beam test in terms of nuclei identification performances of the PSD prototype detector will be shown.

**Index Terms**—Satellite experiments, Plastic scintillator, Silicon Photomultipliers

## I. INTRODUCTION

The High Energy Cosmic Radiation Detection facility (HERD) is one of the cosmic-ray experiments that will be installed onboard the future Chinese Space Station (CSS) providing high quality data on charged cosmic rays in an energy

range from a few GeV to PeV and gamma rays with energy above 100 MeV [1]. One of the instrument subsystem will be the Plastic Scintillator Detector (PSD), which will surround the entire instrument with the main goal of discriminating charged from neutral particles. Plastic scintillators are widely used in satellite experiments as anti-coincidence systems for gamma-ray detection and for the identification of charged cosmic-ray nuclei [2], [3]. For these applications, a high detection efficiency (> 99.9%) is required in order to ensure a high background rejection for the gamma-ray identification and a good charge resolution is also needed to measure the nuclei charge up to iron [4], [5]. The configuration proposed for the HERD PSD consists of trapezoidal scintillator bars coupled to Silicon Photomultipliers (SiPMs). The segmented geometry is necessary to reduce the possible self-veto due to the backsplash effect [6], while the trapezoidal shape is chosen to ensure the best packaging of the whole detector. SiPMs will be adopted to readout the scintillation light instead of the traditional Photomultiplier Tubes (PMTs) currently used in space missions, offering the possibility of more compact and lower power consumption detectors, without any performance loss.

Beam test campaigns at CERN were performed to study the overall performances of the PSD, aiming at the optimization of the scintillator geometry and the SiPM-based readout. In this work the performance of a prototype composed of 8



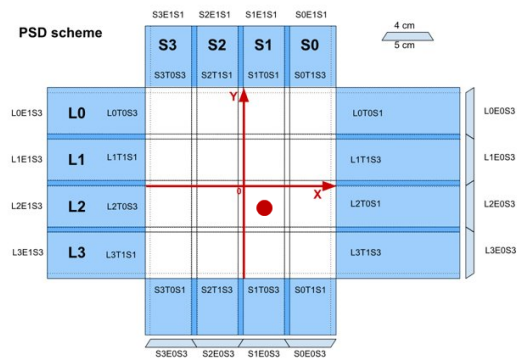


Fig. 3. Schematic of the PSD prototype. Long (40 cm length) and short (30 cm length) bars are named L and S respectively. Each bar is read-out by a PCB with three Hamamatsu  $1.3 \times 1.3 \text{ mm}^2$  S14160-1315 (S1) and three Hamamatsu  $3 \times 3 \text{ mm}^2$  S14160-3015 (S3) SiPMs placed on the larger face of the tile (“top” SiPM, T) and a single  $3 \times 3 \text{ mm}^2$  S14160-3015 SiPM coupled at the two end of the bar (“end-cap”, E). The prototype was irradiated in the position indicated by the red point, between the L2 and the S1 bar.

to readout the SiPMs of the HERD Fiber Tracker (FiT [8]). The main objective of the BETA ASIC is to perform the raw signal amplification and pre-processing with very low power consumption, large dynamic range and good signal-to-noise ratio (SNR) at the single photo-electron level, as required for space applications. The 16-channel ASIC provides the possibility to perform charge measurements with a digitalized serial output. The main characteristics of the ASIC are shown in Tab. II-A.

Channels	16
Input Rate	1 kHz (max recommended)
Power draw	$0.5 \frac{\text{mW}}{\text{ch}}$
Dynamic range	676 MIP (18748 phe) or 12 bits

\*Taken from datasheet [7].

The Front-End architecture is based on a multi-gain system that reads the input current from each SiPM and converts it into voltage. This multi-gain system intends to provide good amplification for low number of photons working with the *High-Gain Amplifier* (HG) and a large dynamic range selecting the *Low-Gain Amplifier* (LG). An automatic path selection comparator allows to switch to LG when the HG dynamic range saturates [7]. In Fig. 2 the block diagram of the BETA ASIC is shown.

### III. BEAM TEST MEASUREMENTS

The PSD prototype was irradiated with an ion beam with selected momentum of 330 GeV/Z, coming from a primary beam of lead, with energy 150 GeV/A, impinging onto a Beryllium target with a size of 4 cm and a  $A/Z = 2.2$  ion selection. The PSD was aligned such that the beam was irradiating a region across the long tile L2 and the short bar S1, as shown in Fig. 3. On the beam axis the two T1 and T2 squared tiles are also placed respectively upstream and downstream the PSD prototype as shown in Fig. 4. This allows to monitor the beam composition and the particle

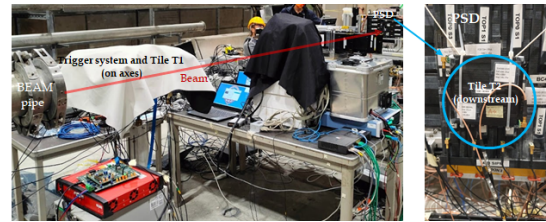


Fig. 4. On the left: Picture of the beam test setup. In order of placement on the beam line: the T1 tile and the trigger system, the PSD prototype and the T2 tile. On the right: a zoom of the PSD with the tile T2 behind the prototype with respect on the beam direction.

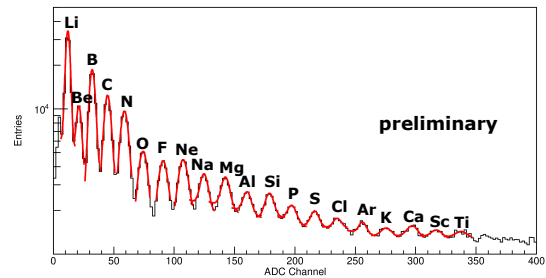


Fig. 5. ADC channel spectrum of the T1-S3 SiPM (Tile T1, upstream the beam). The counts are fitted with a multi-gaussian in order to distinguish between the different nuclei, up to  $Z = 23$ .

fragmentation due to the presence of other subsystems between the beam pipe and the PSD prototype. A trigger system is also used to select the primary particles with  $Z \geq 3$ .

Fig. 5 shows the ADC channel spectrum of the T1-S3 SiPM (upstream tile). The spectrum shows a good charge resolution that allows to distinguish signals generated from nuclei up to  $Z = 23$ . A multigaussian fit is superimposed to the spectrum in order to calculate the charge resolution. On the other hand, the PSD prototype and the T2 tile spectra do not show such a high charge resolution. Fig. 6 shows the spectra of the T1 tile (top panel), T2 tile (central panel) and the PSD L2 bar (bottom panel) obtained by reading the signal both with small and large SiPMs. This different behaviour is due to the particle fragmentation along the beam line that does not allow to resolve peaks for nuclei with  $Z > 6$ .

To infer the signals due to the primary particles with  $Z > 6$ , we correlated events from T1 tile with those from T2 tile and PSD L2 bar. Left panels in Figs. 7 show a two-dimensional scatter plot of these events. The diagonal spots observed in these plots correspond to the primary particle signals, while the tails originating from these spots represent the energy released by daughter particles. Using the multi-gaussian fit performed on the T1 spectrum, we selected the events associated to each primary beam particle. The projection slice of the scatter plot for each primary ion gives the signal observed by the T2 tile and the PSD L2 bar originated from that selected primary ion. In the rights plots on Figs. 7 these spectra are superimposed to the overall count spectra. Each color represent a different primary ion selection. The peak in each spectrum is due to the primary particles reaching the analyzed scintillator without

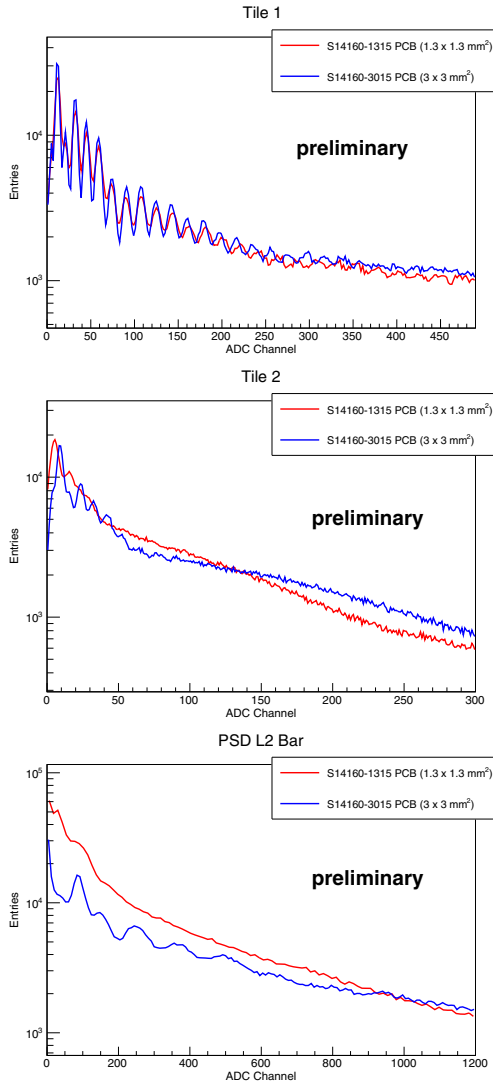


Fig. 6. ADC channel spectra of the Tile T1 (top panel), Tile T2 (central panel) and PSD prototype bar L2 TOP PCBs (bottom panel). The S14160-1315 and S14160-3015 SiPM ADC channels are shown respectively in red and blue.

fragmentation, while the long tails at lower ADC count values represent the energy released by all the daughters generated along the beam line.

With this data selection procedure, we were able to identify the expected peak ADC channel value for the PSD prototype bar.

#### A. Charge resolution measurement

The spectra obtained with the procedure described in previous sections were used to measure the charge resolution and to explore the Birks' saturation effect, which is crucial to correctly calibrate the PSD response. For low energy depositions, the number of photons generated by the scintillation process inside the plastic scintillator (and therefore the ADC signal amplitude read out by the SiPMs) increases linearly with the energy deposited by the primary particles, while for higher

energy losses a saturation effect is commonly observed in plastic scintillator materials. This saturation effect is described by the Birks' law [11]. Since the energy deposited depends on  $Z^2$  of the incoming particle, a correct equalization of the ADC channels for the PSD is crucial to identify the charges of the nuclei in cosmic rays. The Birks' law well describes the photon generation mechanisms in the scintillation region close to the primary energy deposit (so called, scintillation "core"). On the other hand, the scintillation photon production remains still linear in the region far away from the primary energy deposit (scintillation "halo") [9]. In literature, the halo linear behavior is sometimes attributed to  $\delta$ -ray electrons, which deposit their energy far from the primary ionization site. All these mechanisms are taken into account in the "halo-core" quenching effect equation that describes the total scintillation light yield per unit length  $dL/dx$  [9]:

$$\frac{dL}{dx} = A \cdot \frac{(1 - f_h) \cdot \frac{dE}{dx}}{1 + k_b \cdot \frac{dE}{dx}} + A \cdot f_h \frac{dE}{dx} \quad (1)$$

where:

- $dE/dx \propto Z^2$ ;
- $f_h$  represents the fraction of energy deposited in the halo;
- $k_b$  is the Birks constant that depends on the material and governs the strength of the saturation;
- $A$  is an overall gain normalization.

The plot in Fig. 8 shows the ADC counts as a function of  $Z^2$  of the primary particle for the PSD L2 bar. Each point from left to right corresponds to  $\text{Li}^{3+}$ ,  $\text{Be}^{4+}$ ,  $\text{B}^{5+}$ , etc. The red line represents the best-fit curve obtained using Eq. (1), showing a very good agreement with the measured data.

Finally, in order to evaluate the capability of the PSD prototype to identify nuclei, an estimate of the energy resolution is obtained by fitting the peaks corresponding to the different primary  $Z$  particles with a Gaussian function. The energy resolution  $R$  was evaluated as  $R = \sigma/MPV$ , where  $MPV$  and  $\sigma$  are the mean and the sigma of each fitted Gaussian. In the plot in Fig. 9, the  $R$  value as a function of  $Z$  of the primary particle is shown for all the different detector prototypes tested (T1 tile, T2 tile and PSD L2 bar). The second axis on the top of the plot shows also the expected energy released by each ion that is evaluated by means of a Monte Carlo simulation [12], [13]. It is possible to observe that high- $Z$  particles are better resolved. Furthermore, the lower scintillation light collected by small SiPMs (i.e. the S14160-1315 -  $1.3 \times 1.3\text{mm}^2$ ) reduces the energy resolution compared to the larger ones (i.e. the S14160-3015 -  $3 \times 3\text{mm}^2$ ). On the other hand, using small sensors allows to increase the dynamic range of the detector to avoid saturating the readout chain for high- $Z$  particles.

From Fig. 9 it is also possible to observe that the L2 bar and T2 tile have similar charge resolutions. This implies that the geometry of the scintillator material does not affect dramatically the energy resolution of the detector. In addition, top and end-cap SiPMs of the bar shows comparable resolutions, allowing more freedom in the positioning of the

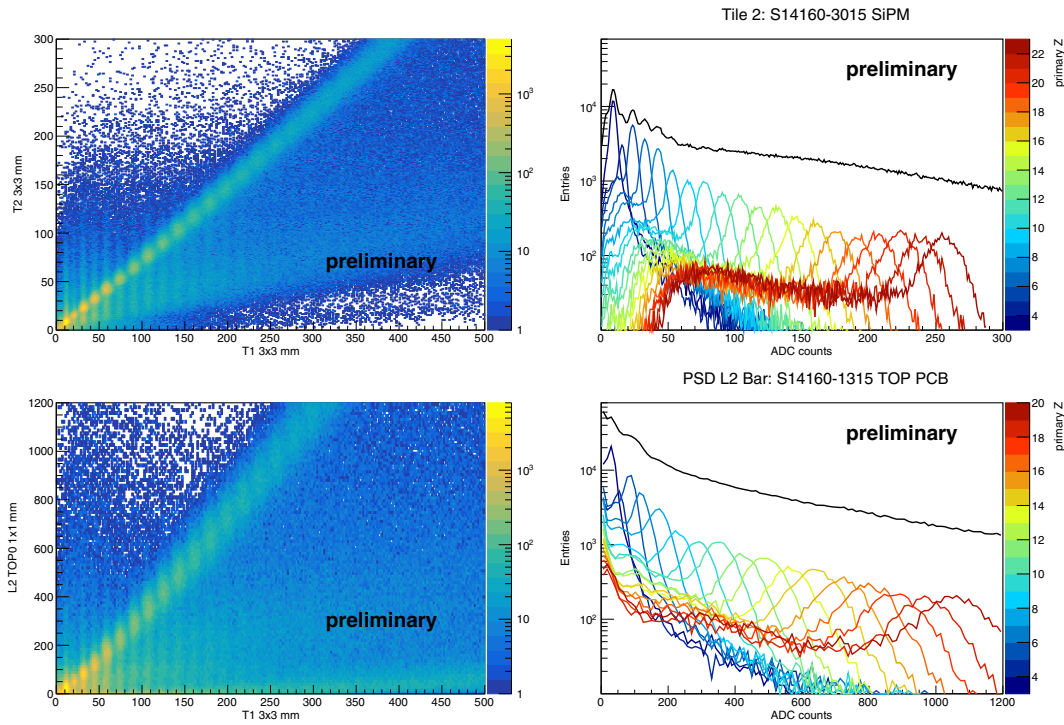


Fig. 7. *Top panel*: Scatter plot with the correlated data of the tile T1 and the tile T2 (top-left panel) and the tile T1 and L2 bar of the PSD prototype (TOP SiPMs -  $3 \times 3$  PCB) (bottom-left panel) Tile T2 (top-right panel) and PSD L2 bar (bottom-right panel) overall spectrum over imposed with the spectra generated by each primary particle. These spectra are inferred by the selection performed from the scatter plots. Each color represent a different primary ion  $Z$ .

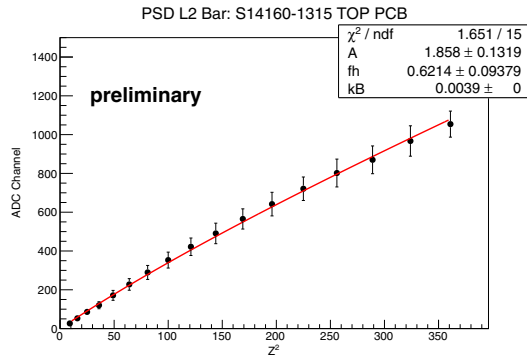


Fig. 8. Mean ADC channels as a function of the  $Z^2$  of the different primary ions from the selected signals of the PSD L2 bar correlated with the T1 tile. The red line represents the best-fit curves obtained using “halo-core” formula (Eq. 1).

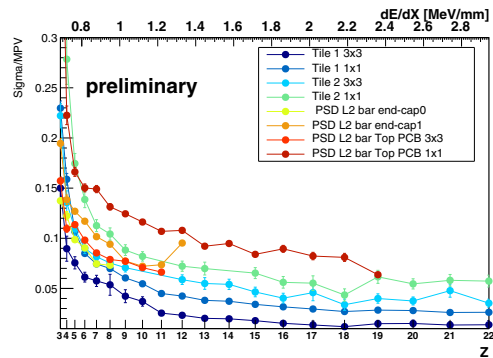


Fig. 9. Resolution evaluated as  $R = \frac{\sigma}{MPV}$  for all the detector tested as a function of  $Z^2$  of the different primary ions and their mean energy released (estimated using a Monte Carlo simulation [12], [13]).

sensors and facilitating the mechanical design and assembly of the PSD. Finally, the PSD bar and the T2 tile show poorer resolutions with respect to T1 tile. This is probably related to the fragmentation effect described in previous sections and suggests that the results obtained for the PSD prototype can be improved if this effect is removed.

## CONCLUSIONS

Plastic Scintillator Detector (PSD) in satellite experiments are used for  $\gamma$ -identification (veto of charged particles) and

nuclei identification (charge measurement). In this work the main results of the SPS H8 beam test performed at CERN to explore the PSD prototype performance identification have been shown. The results obtained can be used to define the final geometry of the PSD of the HERD facility and the best configuration for the SiPM positioning in order to satisfy the requirements to be used as charge detector.

## ACKNOWLEDGMENT

The authors would like to thank all the technical staff of the INFN Bari and in particular M. Papagni, F. Maiorano, N. La-

calamita, M. Franco and S. Martiradonna for their fundamental help in the realization of the prototypes. The authors acknowledge financial support from Grant PID2020-116075GB-C21 funded by MCIN/AEI/ 10.13039/501100011033 and by “ERDF A way of making Europe”.

#### REFERENCES

- [1] Dong, Y. *et al.* “Overall Status of the High Energy Cosmic Radiation Detection Facility Onboard the Future China’s Space Station.” 36th International Cosmic Ray Conference (ICRC2019) 36, pp. 62.
- [2] Moiseev, A. A. *et al.* “The anti-coincidence detector for the GLAST large area telescope”, *Astrop. Phys.* 27, 339 (2007).
- [3] Yu, Y. *et al.* “The plastic scintillator detector for DAMPE”, *Astrop. Phys.* 94, 1 (2017).
- [4] Serini, D. *et al.* “Characterization of plastic scintillators equipped with SiPM for the next generation of satellites for the study of cosmic radiation.” *Il nuovo cimento C* 43.2-3 (2020): 1-2.
- [5] F., Gargano *et al.* “Particle identification capability of Plastic scintillator tiles equipped with SiPMs for the High Energy cosmic-Radiation Detection (HERD) facility.” *Nucl.Instrum. Meth.A* 983 (2020) 164476.
- [6] HU, Peng, *et al.* “A preliminary simulation study of influence of back-splash on the plastic scintillator detector design in HERD experiment.” *Radiation Detection Technology and Methods* (2021) pp. 1-7.
- [7] A. Sanmukh *et al.*, “Fiber Tracker Readout BETA ASIC for the High Energy Cosmic Radiation Detection (HERD) facility” *IEEE Nuclear Science Symposium and Medical Imaging Conference (NSS/MIC)*, Piscataway, NJ, USA, (2021), pp. 1-3.
- [8] Perrina, C., *et al.* “The tracking system of HERD.” 36th International Cosmic Ray Conference (ICRC2019), 36, pp. 122.
- [9] Dwyer, Robert and Zhou, Dazhuang “Plastic scintillator response to relativistic nuclei,  $Z \leq 28$ ”, *Nucl. Instrum. Meth.A* 242 (1985), pp.171-176.
- [10] H. Bethe, J. Ashkin, “Stopping Powers and Ranges for Protons and Alpha.” *Experimental Nuclear Physics*, 64 (1953) 253.
- [11] Birks J.B “Scintillations from organic crystals: specific fluorescence and relative response to different radiations.” *Proc.Phys.Soc.A*, 64 (1951) pp. 874-877.
- [12] Altomare C., Serini D. *et al.* “A full and customizable simulation of a scintillation tile equipped with SiPMs for Plastic Scintillator Detectors in the next generation of satellite experiments.”, *Nucl.Instrum.Meth.A* 982 (2020) 164479.
- [13] Altomare, C., Serini D. *et al.* “A complete MC optical photons tracking simulation of Plastic Scintillator Detectors for the next generation of satellite experiments.” *Journal of Physics: Conference Series*. IOP Publishing, (2022) p. 012050.